Munera, S.; Blasco Ivars, J.; Amigo, J.; Cubero-García, S.; Talens Oliag, P.; Aleixos Borrás, MN. (06-2). Use of hyperspectral transmittance imaging to evaluate the internal quality of nectarines. Biosystems Engineering. 182:54-64. https://doi.org/10.1016/j.biosystemseng.2019.04.001

Use of hyperspectral transmittance imaging to evaluate the internal quality of nectarines

Sandra Munera[a], José Blasco[b], Jose Manuel Amigo[c], Sergio Cubero[d], Pau Talens[e], Nuria Aleixos[f*]

a) Centro de Agroingeniería, Instituto Valenciano de Investigaciones Agrarias (IVIA). Carretera CV-315, Km 10.7, 46113 Moncada, (Spain). munera_san@gva.es

b) Centro de Agroingeniería, Instituto Valenciano de Investigaciones Agrarias (IVIA). Carretera CV-315, Km 10.7, 46113 Moncada, (Spain). blasco_josiva@gva.es

c) Department of Food Sciences, Faculty of Science, University of Copenhagen. Rolighedsvej 30, Frederikberg C DK-1958, (Denmark). jmar@food.ku.dk

d) Centro de Agroingeniería, Instituto Valenciano de Investigaciones Agrarias (IVIA). Carretera CV-315, Km 10.7, 46113 Moncada, (Spain). cubero_ser@gva.es

e) Departamento de Tecnología de Alimentos, Universitat Politècnica de València. Camino de Vera, s/n, 46022 Valencia (Spain). pautalens@tal.upv.es

f) Departamento de Ingeniería Gráfica, Universitat Politècnica de València. Camino de Vera, s/n, 46022 Valencia (Spain). *Corresponding author: naleixos@dig.upv.es Tel.: +34 963879514

ABSTRACT

The internal quality of nectarines (*Prunus persica* L. Batsch var. *nucipersica*) cv. 'Big Top' (yellow flesh) and 'Magique' (white flesh) has been inspected using hyperspectral transmittance imaging. Hyperspectral images of intact fruits were acquired in the spectral range of 630−900 nm using transmittance mode during their ripening under controlled conditions. The detection of split pit disorder and classification according to an established firmness threshold were performed using PLS-DA. The prediction of the Internal Quality Index (IQI) related to ripeness was performed using PLS-R. The most important variables were selected using interval-PLS. As a result, an accuracy of 94.7% was obtained in the detection of fruits with split

pit of the 'Big Top' cultivar. Accuracies of 95.7 % and 94.6 % were achieved in the classification of the 'Big Top' and 'Magique' cultivars, respectively, according to the firmness threshold. The internal quality was predicted through the IQI with R^2 values of 0.88 and 0.86 for the two cultivars. The results obtained indicate the great potential of hyperspectral transmittance imaging for the assessment of the internal quality of intact nectarines.

Keywords: *stone fruit, split pit, ripeness, internal quality, hyperspectral imaging, computer vision*

1. INTRODUCTION

Nectarine (*Prunus persica* L. Batsch var. *nucipersica*) is one of the fruits to which plant breeders have devoted the most effort in recent years in order to improve agronomic performance and enhance their appearance and quality (Iglesias & Echeverría, 2009; Reig, Alegre, Gatius, Iglesias, 2013; Munera et al., 2017). However, this effort has not resulted in an increase in consumption due to the fruit being harvesting too early, which means that the products often lack flavour and have excessive firmness, irregular quality and a lack of product identification (Iglesias & Echeverría, 2009; Munera et al., 2018). Therefore, a prior evaluation of quality would be necessary to offer consumers fruits that best match their preferences. Some of these preferences are related to the ripeness of the fruit when consumed. But the skin colour of red cultivars makes it virtually impossible to visually determine the exact stage of maturity. On the other hand, ripening of peaches and nectarines is related with changes during storage that transform a mature fruit into one that is ready to be eaten (Crisosto, 1994). Therefore, maturity at harvest determines the quality of fruit when it reaches the consumer (Jacob et al., 2006).

Hyperspectral imaging has emerged as a potential and powerful tool for safety and quality inspection of agricultural products (Lorente et al., 2012). This non-destructive technique integrates conventional imaging and spectroscopy to obtain both spatial and spectral information from an object simultaneously, thus making it a useful tool for evaluating individual fruits, vegetables or grains (Qin, Chao, Kim, Lu, Burks, 2013). Most of the hyperspectral imaging systems found in the literature have been implemented to capture images

of the samples illuminated by appropriate lighting systems that make it possible to capture the light reflected by the sample. The differences found between the light emitted by the lamps and the radiation reflected by the samples allows certain attributes related to the composition or the quality to be estimated. Examples are found in vegetables, such as pepper (Schmilovitch et al., 2014), tomato (Liu, Liu, Chen, Yang, Zheng, 2015) or rocket leaves (Chaudhry et al., 2018), cereals, like maize (Williams & Kucheryavskiy, 2016), or rice (Kong, Zhang, Liu, Nie, He, 2013), and fruits such as bananas (Rajkumar, Wang, EImasry, Raghavan, Gariepy, 2012), pears (Li et al., 2016), grapes (Baiano, Terracone, Peri, Romaniello, 2012), strawberries (Zhang et al., 2016) or apples (Baranowski, Mazurek, Pastuszka-Wozniak, 2013). In the case of stone fruit, Herrero-Langreo, Lunadei, Lleó, Diezma and Ruiz-Altisent (2011) assessed the ripeness of peaches by using multispectral indexes; Lu and Peng (2006) assessed the firmness of peaches; Zhu, Lin, Nie, Wu and Chen (2016) obtained firmness distribution maps inside the peach pulp. This technology was also used to monitor the ripeness of two cultivars of nectarines (Munera et al., 2017) and to discriminate between similar cultivars with precision (Munera et al., 2018).

On the contrary, hyperspectral imaging in transmittance mode is more effective in detecting internal defects and concentrations in translucent materials, as is the case of some fruits. When a fruit is illuminated with a strong light, the incident radiation may be reflected, absorbed or transmitted, and the relative contribution of each phenomenon depends on the chemical constitution and physical parameters of the sample (Nicolaï et al., 2007). The transmission mode may be less susceptible to surface properties and hence better for detecting composition or internal disorders than the reflectance mode (Schaare & Fraser, 2000). When this mode is used in hyperspectral imaging, the camera is located on the opposite side to the light source and captures the light transmitted through the sample. Transmittance has already been used to analyse the mechanical properties of blueberries (Leiva-Valenzuela, Lu & Aguilera, 2014; Hu, Dong, Liu, Opara & Chen, 2015), and to detect pits in cherries (Qin & Lu, 2005; Siedliska, Baranowski, Zubik & Mazurek, 2017), defects in pickling cucumbers (Cen, Lu, Ariana & Mendoza, 2014) and damage in soybeans (Huang, Wan, Zhang & Zhu, 2013). However, to our knowledge, no previous works have been undertaken to study the application of hyperspectral

imaging in transmittance mode in stone fruit such as nectarines. This technique could be an interesting alternative to evaluate their physicochemical properties but also important disorders such as split pit (Figure 1). This phenomenon consists in the splitting of the pit along the suture/seam of the endocarp, resulting in the two halves of the endocarp being detached from each other inside the mesocarp.

When this disorder happens, the fruit generally develops rot problems far more quickly than sound fruit, and there is a higher risk of the disease spreading more rapidly from split pit fruit to other fruit during the postharvest operations of storage or marketing (Tani, Polidoros & Tsaftaris, 2007). In most cases, even in the most advanced cases, no visual symptoms of pit splitting or breakage can be observed, and it is only detected when the fruit is opened (Kritzinger, Lötze & Jooste, 2017). This can be a big problem in nectarines because it can affect 45% of the fruits, depending on the cultivar and the season (IRTA, 2016). Therefore, non-destructive techniques such as computed tomography (Kritzinger et al., 2017), X-ray (Han, Bowers & Dodd, 1992) or, more recently, acoustic vibration methods (Nakano et al., 2018) have been used in an attempt to detect this problem in plums and peaches.

The aim of this work is to investigate the potential use of hyperspectral imaging in transmittance mode as a tool for the non-destructive evaluation of the internal quality of two cultivars of nectarine. This quality evaluation is related to the detection of fruit with split pit and to the ripeness monitoring determined by two indicators, the internal quality index, IQI, and a firmness threshold (35 N).

2. MATERIAL AND METHODS

2.1 Fruit samples

This study was performed in parallel to a previous work in which the ripeness of ‘Big Top’ (yellow flesh cultivar) and ‘Magique’ (white flesh cultivar) nectarines was monitored using hyperspectral imaging in the reflectance mode (Munera et al., 2017).

In this case, a total of 168 fruits of each cultivar, ‘Big Top’ and ‘Magique’, were harvested in a commercial orchard in Lerida (Spain) in the commercial maturity period. The fruits of each

cultivar were grouped in batches of 28 fruits and stored under controlled conditions (15 ºC, 90 % relative humidity) until senescence. The image acquisition and the analyses of the 'Big Top' cultivar were performed before storage and then on the 1st, 2nd, 3rd, 5th and 8th days; for 'Magique' nectarines they were performed before storage and then on the 2nd, 4th, 7th, 10th and 14th days. Different days were selected for the analyses due to different ripening speeds for each cultivar (Munera et al., 2017).

Initially, all of the fruits presented a sound appearance and there were no external signs of split pit in any of them. The experiments to detect this disorder were carried out after the image acquisition. A total of 137 'Big Top' fruits presented a normal pit and 31 (18.5%) were identified as split pit (Figure 1). In the case of the 'Magique' cultivar, no fruits presented split pit.

2.2 Hyperspectral transmittance image acquisition and processing

The hyperspectral imaging system used to acquire the images in transmittance mode (Figure 2) was composed of an industrial camera (CoolSNAP ES, Photometrics, AZ, USA), coupled to two liquid-crystal tuneable filters (LCTF) (Varispec VIS-07 and NIR-07, Cambridge Research & Instrumentation, Inc., MA, USA). A lens capable of maintaining the focus across the full spectral range (Xenoplan 1.4/23, Schneider Optics, Hauppauge, NY, USA) was also used. The camera was configured to acquire images with a size of 1392×1040 pixels and a spatial resolution of 0.14 mm/pixel. The camera and the filters are sensitive in the range from 400 to 1100 nm. However, little light crosses the nectarines and the images appeared very dark when the time of the light exposition was limited to no more than 10 s per wavelength in order to avoid any damage in the fruit. Therefore, a calibration was carried out so that the integration time was increased as much as possible while ensuring that the maximum intensity (saturation) was not reached for any wavelength in any region of the image. To avoid the low sensitivity of the sensors close to the edges of this range, the images were captured at every 10 nm in the working spectral range of 630 nm−900 nm, resulting in 28 images obtained at different

wavelengths. This is in accordance with Qin and Lu (2005), who selected the spectral range from 692 to 856 nm to detect pits in cherries using transmittance.

The fruit was placed manually in a holder with a foam foil located between the camera and the illumination system in which the fruit was inserted to ensure that only the light that was transmitted through the fruit reached the camera (Figure 2). The nectarines were oriented so that the pedicel was pointing downwards and directly illuminated by the twelve halogen spotlights (37 W) (Eurostar IR Halogen MR16. Ushio America, Inc., CA, USA) powered by direct current (12 V). The lamps were arranged equidistant from each other outside a hemispherical aluminium diffuser (Figure 2).

In order to extract the actual response of the samples at each wavelength, while avoiding light-dependent intensities, a correction was applied. Several methods have been described to correct the effect of the spectrum of the light source in transmittance mode, from no correction (Siedliska et al., 2017), which is clearly wrong, to the use of different materials, such as opal glass, or measuring the light source directly with no samples (Cogdill, Hurburgh & Rippke, 2004; Ariana & Lu, 2008). This last option is actually equivalent to correcting the images using the reflectance of a standard white reference. A correction was then performed using the image of a standard white reference (Spectralon 99%, Labsphere, Inc, NH, USA) captured with a reduction in the integration time to prevent saturation (Gomez-Sanchis et al., 2014). The influence of the minimum dark current of the camera was also captured by switching off the lamps and placing a cap in the lens to prevent the light from getting inside the camera. The correction was performed using the correction in Equation 1:

$$I = \frac{I_0 - I_{black}}{I_{white} - I_{black}} \quad (1)$$

where I_0 is the raw acquired image of the fruit, I_{white} is the image of the standard white reference, and I_{black} is the image acquired while avoiding any light source. The images obtained were

processed using the toolbox HYPER-Tools (Mobaraki & Amigo, 2018) for MATLAB R2017b (The MathWorks, Inc. MA, USA).

As Ariana and Lu (2008) pointed out, transmittance is affected by the diameter of the fruit, and therefore the effect of the fruit size was corrected using Equation 2:

$$I_d = \frac{I \, x \, d_n}{d_t} \quad (2)$$

where I is the corrected image obtained previously, d_n is the diameter of the individual fruit and d_t is the average of the diameters of all the fruits of each cultivar.

Finally, the mean transmittance spectrum was obtained by averaging the relative transmittance spectra without including the possible saturated pixels on the edge of the fruit (Figure 3). A total of 168 mean spectra representing the fruits of each cultivar (28 mean spectra per five days of analysis) were obtained for assessment of their internal quality by means of multivariate data analysis methods. In the case of 'Big Top' cultivar, 137 mean spectra corresponded to fruits with normal pit and 31 with split pit.

2.3 Reference quality parameters

The determination of reference quality parameters was performed after image acquisition on each day of analysis in order to monitor the ripening of both cultivars of nectarines.

The analysis of the flesh firmness (F) was performed using a texturometer (XT2 Stable, MicroSystems Haslemere, UK) equipped with a 6 mm flat plunger. The crosshead speed during the puncture test was 1 $mm.s^{-1}$. The maximum force, expressed in N, was registered on opposite sides of the fruits.

The colour of the flesh was obtained using a colorimeter (MINOLTA CM-700D, Minolta Co. Tokyo, Japan) with the standard illuminant D65 and the CIE standard observer 10°. Luminosity (L^*), chroma (C^*) and hue (h^*) parameters were obtained in the CIELCh colour space. The total soluble solids (TSS) value was analysed from the juice of each nectarine with a

digital refractometer (RFM330+VWR, Internacional Eurolab S.L., Barcelona, Spain) at 20 °C and the results were expressed as a percentage of the TSS.

The internal quality index (IQI) was calculated using Equation (3) (Cortés et al., 2016). This index relates internal physicochemical properties to a sensory perception of its ripeness.

$$IQI = \ln \frac{100 \times F \times L^* \times h^*}{TSS \times C^*} \quad (3)$$

The analysis of variance (ANOVA), followed by Tukey's Honestly Significant Difference (HSD) test was conducted to determine significant differences (significance defined at $p\text{-}value \leq 0.05$) in the reference properties of the fruit during the ripening process using the software Statgraphics (Manugistics Corp., Rockville, USA).

2.4 Multivariate data analysis

In this work, the prediction of the ripeness properties by means of the IQI was performed using models based on partial least squares regression (PLS-R) and the discrimination between split and normal pit and the corresponding F was carried out by means of models based on partial least squares discriminant analysis (PLS-DA).

PLS-R searches for a linear regression model of latent variables by projecting prediction variables *X* and response variables *Y* into a new latent space where the covariance between these latent variables is maximised. In this work, the goal is to find the latent multidimensional direction in the wavelengths space that explains the direction of the maximum multidimensional covariance in the reference parameter space (Lorente et al., 2012).

In PLS-DA the *Y* variable is categorical, expressing the class membership of the samples. It is performed in order to sharpen the separation between groups of observations by maximising the covariance between the wavelengths and the classes, such that a maximum separation among these classes is obtained (Lorente et al., 2012).

All models were calibrated using the mean transmittance spectra of two thirds of the fruit and later validated using the remaining third. For the detection of split pit, the mean transmittance spectra of 92 fruits with normal pit and 20 with split pit were used as a training set to calibrate the model, and the remaining spectra of 45 fruits with normal pit and 11 with split pit were used as a test set to validate the model. Both the fruits in the calibration and the validation sets were selected with different degrees of ripeness. In the case of ripeness monitoring, the models for 'Big Top' were calibrated using the mean transmittance spectrum of 92 fruits and validated using 45 (removing split pit fruits). The models for 'Magique' were calibrated using the mean spectra of 112 fruits and validated using 56.

All spectra were previously pre-processed using standard normal variate (SNV) to remove the scatter and then normalised using mean-centering (Rinnan, van den Berg & Engelsen, 2009). A 10-fold cross-validation was used to choose the optimal number of latent variables (LV) as well as to obtain an estimation of the error rate of the models. The accuracy of the PLS-R models and predictive capability were evaluated by the coefficient of determination (R^2) and the root mean squared error (RMSE) between the predicted and the measured values of the reference parameter for calibration, cross validation (CV) and prediction. Furthermore, the ratio of performance to deviation (RPD), defined as the ratio between the standard deviation of the reference data and RMSEP, was used (Williams, 1987). The results of the PLS-DA models were expressed as a percentage of correct classification and total accuracy for calibration, CV and prediction.

2.5 Selection of optimal wavelengths

Since hyperspectral images have a high dimensionality, which makes it almost impossible to develop automatic inspection systems capable of working in-line or in real time, it is necessary retain the most original information in a few bands, while preserving the greatest amount of variability and the most significant information (Du and Sun, 2006). The interval PLS (i-PLS) algorithm was performed to select the optimal wavelengths in order to detect normal and split pit fruits, classify them according to the firmness threshold and predict the IQI.

This is a method proposed by Nørgaard et al. (2000), in which the whole spectrum is split into equidistant subintervals and models are calculated for each of these intervals (spectral regions). This method performs a sequential search for the best wavelength or combination of wavelengths. It can be performed in either forward or reverse mode, where intervals are successively included or removed from the analysis, respectively. In this case, the forward i-PLS was applied to the training set automatically using the same number of LV as the PLS-R and PLS-DA models, and each interval corresponded to an individual wavelength. The multivariate data analysis was performed using the PLS_Toolbox (Eigenvector Research Inc., USA) working under MATLAB (R2017b, The MathWorks, Inc. MA, USA).

3. RESULTS AND DISCUSSION

3.1 Detection of split pit fruit

The presence of split pit allows the light to cross through the stone fruit without any interference along the suture of the fruit (Figure 3-C). Therefore, the SNV pre-treated mean spectra of both types of fruit followed a very different pattern, as Figure 4 shows.

The discrimination between normal and split pit fruit was performed by means of PLS-DA. The model was built using all of the 28 wavelengths in the spectral range 630–900 nm and calibrated using three LV. In the calibration of the model, a total accuracy of 94.6% was obtained, 95.0% of normal pit and 93.4% of split pit fruits being classified correctly. In the prediction of the test set, a total accuracy of 93.0% was obtained, 91.3% of normal pit and 100% split pit being classified correctly (Table 1).

As commented earlier, no studies have been performed to detect split pit using hyperspectral imaging. However, Qin and Lu (2005) used this technology to detect the presence of pits in cherries and achieved similar results, an accuracy of 96.5%. Other techniques have already been used with the aim of detecting split pit disorder. Han, Bowers and Dodd (1992) used X-ray images and obtained a total classification accuracy of 95.5% using 94 normal pit fruits, 5 cracked and 99 split pit of different cultivars of peach. An acoustic vibration method developed by Nakano et al. (2018) obtained a total classification accuracy of 97.8% using 256

normal pit fruits and 57 split pit in the same cultivar and stage of ripeness. Comparing these results with hyperspectral transmittance imaging, it can be stated that this technology is a feasible alternative for the detection of split pit, especially taking into account the high accuracy in identifying fruits with split pit that was achieved regardless of the stage of ripeness.

To select the optimal wavelengths, the forward i-PLS method was used. This method has been previously used to select the optimal wavelengths in the detection of early bruise on apples (Ferrari et al., 2015) or to asses the internal quality of blueberries (Leiva et al., 2014). Usually, the selection of these wavelengths would be based on the physicochemical properties of the fruit, however in this case is based on which wavelengths transmit more or less light due to the presence of normal or split pit. In this case, 7 optimal wavelengths were selected (630, 670, 680, 700, 740, 800 and 870 nm) which are those that present more differences along the transmittance mean spectrum of both types of fruit (Figure 4). Therefore, a new PLS-DA model was developed with these wavelengths, also calibrated using 3 LVs. However, the results (Table 1) were better than those obtained using the full spectrum for all the testing sets. Thus, the total accuracy in the calibration rose from 94.6% using all the wavelengths to 97.3% and in the classification of the test set, it increased from 93.0% to 94.7%.

Table 1. Results of the detection of split and normal pit fruits of the 'Big Top' cultivar using all the selected wavelengths.

			Calibration				Cross validation				Prediction			
#V	#LV	Class	NP	SP	CC (%)	A (%)	NP	SP	CC (%)	A (%)	NP	SP	CC (%)	A (%)
28	3	NP	90	1	98.9	98.2	85	6	93.4	94.6	42	4	91.3	93.0
		SP	1	19	95.0		1	19	95.0		0	11	100	
7	3	NP	91	0	100	99.1	89	2	97.8	97.3	43	3	93.5	94.7
		SP	1	19	95.0		1	19	95.0		0	11	100	

#V=number of variables; #LV=number of latent variables; NP = normal pit; SP = split pit; CC = correct classification; A = accuracy.

3.2 Ripeness monitoring

3.2.1 Analysis of the reference parameters and spectral information

Figure 5 shows the evolution of the physicochemical properties measured in fruits of the 'Big Top' and 'Magique' cultivars throughout the experiment. In the case of 'Big Top', these properties were measured only in fruits with a normal pit. The F decreased from 46.3 N to 10.1 N for 'Big Top' and from 57.9 N to 6.1 N for 'Magique'. As stated by Munera et al. (2017), these changes are due to pectin solubilisation and degradation by enzymes acting on the cell walls, whose activity results in a large decline in firmness. Valero, Crisosto and Slaughter, (2007) found that fruits below 35 N could be considered as 'ready to buy' because they are susceptible to damage during postharvest handling, while fruits above this firmness were less susceptible to bruising but could be either mature or immature. This F threshold was therefore selected to classify the fruit because it indicates changes during postharvest ripening and the susceptibility to damage by bruising (Crisosto, Slaughter, Garner & Boyd, 2001).

Regarding the colour of the flesh, both cultivars obtained similar L^* values at the beginning of the experiments, but 'Big Top' underwent a higher reduction in this parameter as the fruit ripened, which is related to a reduction in the brightness perceived during the maturation process. In contrast, 'Magique' presented higher values of h^*, starting with a green colour and eventually reaching a greenish-yellow colour. On the other hand, the fruits from cv 'Big Top' changed from greenish yellow at the beginning to yellow. In the case of C^*, no progressive evolution was observed in either cultivar, but 'Big Top' presented higher values, which means that the colouration was more intense in this cultivar.

The TSS obtained for the 'Big Top' cultivar increased from 10.1 % to 15.1 % on the fifth day, and then dropped to 12.1 % due to over-ripeness. In the case of 'Magique', these values did not change significantly until the last day, when the fruits could be considered over-ripe.

The IQI decreased during fruit ripening for both cultivars, mainly due to the progressive decrease in F and the colour parameters L^* and h^* and the increase in TSS (Figure 5), which is in agreement with Munera et al. (2017). As they pointed out, IQI is more suitable for use as a

standard index on an inspection line because obtaining the reference parameters requires less time and costs.

Figure 6 shows the average transmission spectra of both nectarine cultivars pre-processed using SNV on the different days of postharvest storage. Both cultivars followed a similar spectral pattern during ripeness. The main differences between the days of analysis are observed in the region 630–750 nm for 'Big Top' and also 820–900 nm for 'Magique'. In both cultivars, as the fruits ripen more light is transmitted in the VIS region around 670 nm because the chlorophyll content decreases. In contrast, in the NIR region, the transmission of light is lower in the ripest fruits, probably because the effective absorption bands related to water (OH) and sugar (CH) bonds are relatively wide, partially covering this range (Golic et al., 2003).

3.2.2 Prediction of the Internal Quality index (IQI)

With the aim of predicting the IQI and monitoring the ripeness of both cultivars, a PLS-R model was performed for each cultivar using all 28 wavelengths in the spectral range 630−900 nm.

The optimal model was chosen when the number of LV yields the lowest RMSE for calibration and CV. As Table 2 shows, the calibration of the prediction models was performed using 9 LVs and 7 LVs for the 'Big Top' and 'Magique' cultivars.

In 'Big Top', the R^2 and RMSE values in the calibration were 0.88 and 0.33, and for 'Magique' 0.88 and 0.44, respectively. Regarding the prediction of the test set, the R^2 and RMSE values for 'Big Top' were 0.89 and 0.34, and for 'Magique' 0.88 and 0.43, respectively.

The value of RPD was 2.7 for 'Big Top' and 2.8 for the 'Magique' cultivar. According to Williams (1987), RPD values between 2 and 2.5 indicate that coarse quantitative predictions are possible and a value above 2.5 means good to excellent prediction accuracy. Taking into consideration these values, IQI prediction was excellent for both cultivars (Table 2).

Table 2. Results of prediction of internal quality index (IQI) using all the wavelengths.

Cultivar	#LV	Calibration		Cross validation		Prediction		RPD
		R^2	RMSE	R^2	RMSE	R^2	RMSE	
'Big Top'	9	0.93	0.25	0.88	0.33	0.89	0.34	2.7
'Magique'	7	0.90	0.38	0.88	0.44	0.88	0.43	2.8

#LV = number of latent variables; R^2 = coefficient of determination; RMSE = root mean square error; RPD = ratio of performance to deviation

Munera et al. (2017) achieved an R^2 of 0.89 for both cultivars to estimate the IQI using hyperspectral reflectance imaging on the same sets of fruits. The RMSE in the prediction was 0.33 and 0.44 for 'Big Top' and 'Magique', while the RPD achieved was 3.0 and 2.7, respectively. Therefore, transmittance imaging also has a great potential to obtain and estimate the stage of ripeness of nectarines, but it is not greater than reflectance imaging. The selection of one or the other mode would therefore depend on the application (i.e. split pit can only be detected by transmittance).

3.2.3 Classification according to firmness

In order to discriminate the fruits using the selected F threshold (35 N) between 'ready to buy' (F < 35 N) and 'hard' fruit (F > 35 N), a PLS-DA model was performed for each cultivar. The models were built using all captured wavelengths of the spectral range 630–900 nm.

The model for the 'Big Top' cultivar was calibrated using 4 LVs, obtaining a total accuracy of 95.7 % in the prediction set. The correct classification of 'ready to buy' fruit was 100 % while 93.1 % of 'hard' fruits were classified correctly. In the case of the 'Magique' cultivar, the model was calibrated using 5 LVs, obtaining an overall classification of 94.5 % which is slightly lower than for 'Big Top'. For this cultivar, 90.9 % of 'ready to buy' fruits and 95.7 % of 'hard' fruits were classified correctly. Complete results for all sets are described in Table 3.

Table 3. Results of classification of both cultivars of nectarine by firmness and at all wavelengths.

Cultivar	#LV	Class	Calibration				Cross validation				Prediction			
			H	RB	CC (%)	A (%)	H	RB	CC (%)	A (%)	H	RB	CC (%)	A (%)
'Big Top'	5	H	32	2	94.1	96.7	32	2	94.1	94.5	17	0	100	95.7
		RB	1	56	98.3		3	54	94.7		2	27	93.1	
'Magique'	4	H	35	3	92.1	90.2	35	3	92.1	89.3	22	1	95.7	94.5
		RB	8	66	89.2		9	65	87.8		3	30	90.9	

#LV=number of latent variables; H = *'hard', RB = 'ready to buy'; CC = correct classification; A = accuracy.*

3.2.4 Selection of the optimal wavelengths

The i-PLS algorithm was also applied to the models created to predict both IQI and F. Since most of the wavelengths selected by i-PLS were common for the two quality indicators, only one set of wavelengths per variety was selected to estimate both. Therefore, 13 optimal wavelengths were used to build the models of 'Big Top' (630, 640, 660–690, 710–730, 800, 810, 890 and 900 nm) and 9 for the 'Magique' cultivar (630–690, 890 and 900 nm). Despite the two cultivars analysed in this study are different in the colour of the flesh and in the ripeness pattern, most of selected wavelengths for both cultivars are located in the VIS region (630-690) nm) where carotenoids, chlorophylls and other pigments responsible for fruit colour (Rajkumar et al., 2012). In the case water absorption, several wavelengths were select around 750 nm (first overtone of OH) (710-730 nm) for 'Big Top' and others were selected at the beginning of the spectral valley around 970 nm (third overtone of OH) (890-900 nm) for both cultivars. The wavelengths selected around 850 nm (800-810 nm) are assigned usually to the absorption of acids and sugars (Yang et al., 2015).

For the evaluation of IQI, the PLS-R models were calibrated using 8 and 5 LVs for 'Big Top' and 'Magique' (Table 4). The results obtained in the calibration of the model and prediction of the test set were similar to those using all the wavelengths for 'Big Top' cultivar but were improved in the case of 'Magique' cultivar (Table 2). The values of R^2 of 0.91 and

0.89 and RMSE of 0.29 and 0.41 were obtained in the calibration (CV) of 'Big Top' and 'Magique'. For the prediction of the test set, values of. In this cas,e the RPD values were 2.7 and 3.0.

Table 4. Results of prediction of the internal quality index (IQI) using the selected wavelengths.

Cultivar	#V	#LV	Calibration		Cross validation		Prediction		
			R^2	RMSE	R^2	RMSE	R^2	RMSE	RPD
'Big Top'	13	8	0.93	0.25	0.91	0.29	0.88	0.35	2.7
'Magique'	9	5	0.90	0.37	0.89	0.41	0.89	0.40	3.0

#V = number of variables; #LV = number of latent variable; R^2 = coefficient of determination; RMSE = root mean square error; RPD = ratio of performance to deviation

To classify the fruit by F, the PLS-DA models created using the selected wavelengths were calibrated using 5 LVs for 'Big Top' and 2 LV for 'Magique' (Table 5).

Table 5. Results of classification of both cultivars of nectarine by firmness using a threshold and the selected set of wavelengths.

	#V	#LV	Class	Calibration				Cross validation				Prediction			
				H	RB	CC (%)	A (%)	H	RB	CC (%)	A (%)	H	RB	CC (%)	A (%)
BT	13	5	H	31	3	91.2	94.5	32	2	94.1	93.4	17	0	100	95.7
			RB	2	55	96.5		4	53	93.0		2	27	93.1	
M	9	2	H	37	1	97.4	91.1	36	2	94.7	90.2	23	0	100	94.6
			RB	9	65	87.8		10	64	86.5		3	30	90.9	

BT = 'Big Top'; M = 'Magique'; #V=number of variables; #LV=number of latent variables; H = *'hard', RB = 'ready to buy'; CC = correct classification; A = accuracy.*

As in the case of using all the wavelengths (Table 3), the model for 'Big Top' obtained a total accuracy of 95.7 % in the prediction set. The correct classification of fruits as 'ready to buy' was 100 % while 93.1 % of 'hard' fruits were classified correctly. In the case of the 'Magique' cultivar, the model achieved an overall classification of 94.6 %. For this cultivar,

90.9 % ‘ready to buy’ and 100 % ‘hard’ fruits were classified correctly. The results obtained using the selected set of wavelengths were very similar to those obtained with all the captured wavelengths. Complete results for all sets are described in Table 5.

3.4 Hierarchical classification

With the aim of obtaining the total internal quality of the ‘Big Top’ nectarines at the same time, including both the detection of split pit disorder and the stage of ripeness, a hierarchical model was built using the PLS-DA models previously calibrated with the optimal wavelengths. The class of each fruit in the test set was predicted by introducing the mean spectrum measured into the hierarchical model. The result can be seen in Figure 7, which shows the fruit coloured in black if the mean value was assigned by the model to the split pit class, dark blue if it was assigned to ‘hard’ fruit with normal pit or light blue if it was assigned to the ‘ready to eat’ and normal pit class. In this case, all the split pit and ‘hard’ fruits with normal pit were correctly classified, these results being the same as those obtained by the individual models (Tables 1 and 5). However, three ‘ready to buy’ fruits with normal pit were classified as defective, which may be due to the fact that riper fruit can transmit more light than less ripe fruits. Two other ‘ready to buy’ fruits were classified as ‘hard’.

Hierarchical models has been also used by Bonifazi, Capobianco and Serranti (2018) in order to recognise low-density and high-density polyethylene in mixed plastic waste using hyperspectral imaging. As these authors also pointed out, a hierarchical model allows recognizing different classes under study in a single step, making hyperspectral imaging an even more practical tool for quality control of nectarines.

4. CONCLUSIONS

This paper presents a new approach for the evaluation of the internal quality of nectarines by means of hyperspectral imaging. The transmittance mode was evaluated as a potential non-destructive method to detect split pit fruits and to monitor their ripeness using two quality indicators. The detection of split pit fruits of the ‘Big Top’ cultivar using PLS-DA was

successful, achieving a 100 % correct classification for split pit fruit and 91.3 % for normal pit using all the captured wavelengths. The ripeness of the 'Big Top' and 'Magique' cultivars was determined by two indicators: the ripening index, IQI, and an F threshold (35 N) that is based on the susceptibility to suffer damage by bruising. The prediction of the IQI was performed by means of PLS-R models, obtaining an R^2 of 0.89 and 0.86 and an RPD of 2.7 and 2.6 for the 'Big Top' and 'Magique' cultivars. The classification of the fruits by F was performed by PLS-DA, which correctly classified 95.7 % of the 'Big Top' fruits and 94.5% of the 'Magique' fruits.

To reduce the huge amount of data captured by the hyperspectral imaging system, an optimal wavelength selection was performed by means of forward i-PLS. Thus, the simplified models obtained similar results to those models that used all the wavelengths. Finally, a hierarchical model was built to evaluate the total internal quality of the 'Big Top' cultivar in one step. The prediction was visualized on the fruit surface, indicating that 10.3 % of 'ready to buy' fruits were classified as split pit and 6.9 % as 'hard'.

These results confirm the great potential of this technique to evaluate the internal quality of these two cultivars of nectarine, especially to detect internal defects such as split pit disorder. Nevertheless, this method should be tested in other cultivars and on a larger sample set of fruits grown in different areas and seasons before it can be implemented in an in-line system. Furthermore, the development of a transmission system must take into account the fact that, in order to detect split pit fruits, the fruit must be oriented such that light penetrates through the fruit from the pedicel to the back and the time of the light exposure must be limited in order to avoid any damage to the fruit.

ACKNOWLEDGEMENTS

This work was partially funded by INIA and FEDER funds through project RTA2015-00078-00-00. Sandra Munera thanks INIA for the FPI-INIA grant num. 43 (CPR2014-0082), partially supported by European Union FSE funds.

REFERENCES

Ariana, D.P. & Lu, R. (2008) Quality evaluation of pickling cucumbers using hyperspectral reflectance and transmittance imaging: Part I. Development of a prototype. *Sensing and Instrumentation for Food Quality and Safety 2*, 144–151.

Baiano, A., Terracone, C., Peri, G. & Romaniello, R. (2012). Application of hyperspectral imaging for prediction of physico-chemical and sensory characteristics of table grapes. *Computetrs and Electronics in Agriculture 87*, 142-151.

Baranowski, P., Mazurek, W. & Pastuszka-Wozniak, J. (2013). Supervised classification of bruised apples with respect to the timeafter bruising on the basis of hyperspectral imaging data. *Postharvest Biology and Technology 86*, 249- 258.

Bonifazi, G., Capobianco, G., & Serranti, S. (2018). A hierarchical classification approach for recognition of low-density (LDPE) and high-density polyethylene (HDPE) in mixed plastic waste based on short-wave infrared (SWIR) hyperspectral imaging. Spectrochimica Acta Part A: Molecular and Biomolecular Spectroscopy 198, 115-122.

Cen, H., Lu, R., Ariana, D.P. & Mendoza, F. (2014). Hyperspectral imaging-based classification and wavebands selection for internal defect detection of pickling cucumbers. *Food Bioprocess Technology 7*, 1689–1700.

Chaudhry, M.M.M., Amodio, M.L., Baballahi, F., de Chiara, M.L.V., Amigo, J.M., Colelli, G. (2018). Hyperspectral imaging and multivariate accelerated shelf life testing (MASLT) approach for determining shelf life of rocket leaves. *Journal of Food Engineering 238*, 122-133.

Cogdill, R., Hurburgh, C. & Rippke G. (2004). Single-kernel maize analysis by near-infrared hyperspectral imaging. *Transactions of the ASAE*, 47, 311-320

Cortés, V., Ortiz, C., Aleixos, N., Blasco, J., Cubero, S. & Talens, P. (2016). A new internal quality index for mango and its prediction by external visible and near-infrared reflection spectroscopy. *Postharvest Biology and Technology 118*, 148-158.

Crisosto C.H. (1994). Stone fruit maturity indices: a descriptive review. *Postharvest News and Information*, 5, 65-68.

Crisosto, C.H., Slaughter, D., Garner, D., & Boyd J. (2001). Stone fruit critical bruising thresholds. *Journal of the American Pomological Society 55*, 76-81

Du, C. J. & Sun, D. W. (2006). Learning techniques used in computer vision for food quality evaluation: A review. *Journal of Food Engineering 72*, 39-55.

Ferrari, C., Foca, G., Calvini, R. & Ulrici, A.(2015). Fast exploration and *classification of large hyperspectral image datasets for early bruise detection on apples. Chemometrics and Intelligent Laboratory Systems 146*, 108–119

Golic, M., Walsh, K., & Lawson, P. (2003). Short-wavelength near-infrared spectra of sucrose, glucose, and fructose with respect to sugar concentration and temperature. *Applied Spectroscopy*, 57, 139-145

Gómez-Sanchis, J., Lorente, D., Soria-Olivas, E., Aleixos, N., Cubero, S., & Blasco, J. (2014) Development of a hyperspectral computer vision system based on two liquid crystal tuneable filters for fruit inspection. Application to detect citrus fruits decay. *Food and Bioprocess Technology*, 7, 1047-1056.

Han, Y.J., Bowers & S. V., Dodd, R.B. (1992). Nondestructive detection of Split-pit peaches. *Transactions of the ASAE 35*, 2063-2067.

Herrero-Langreo, A., Lunadei, L., Lleó, L., Diezma, B. & Ruiz-Altisent, M. (2011). Multispectral vision for monitoring peach ripeness. *Journal of Food Science 2*, 178-187

Hu, M.H., Dong, K.L., Liu, B. L., Opara, U.L. & Chen, L. (2015) Estimating blueberry mechanical properties based on random frog selected hyperspectral data. *Postharvest Biology and Technology 106*, 1-10

Huang, M., Wana, X., Zhang, M. & Zhu, Q. (2013). Detection of insect-damaged vegetable soybeans using hyperspectral transmittance image. *Journal of Food Engineering 116*, 45–49

Iglesias, I. & Echeverría, G. (2009). Differential effect of cultivar and harvest date on nectarine colour, quality and consumer acceptance. *Scientia Horticulturae 120*, 41-50.

Institut de Recerca i Tecnologia Agroalimentàries (IRTA). (2016). XX Exposición de variedades de melocotón y nectarina. http://kp.eufrin.eu/ Accessed 03/11/18

Jacob, S., Vanoli, M., Grassi, M., Rizzolo, A., Eccher Zerbini, P., Cubeddu, R., Pifferi, A., Spinelli, L., & Torricelli A. (2006). Changes in sugar and acid composition of 'Ambra' nectarines during shelf life based on non-destructive assessment of maturity by time-resolved reflectance spectroscopy. *Journal of Fruit and Ornamental Plant Research*, 14, 183-194

Kong, W., Zhang, C., Liu, F., Nie, P. & He, Y. (2013). Rice seed cultivar identification using near-infrared hyperspectral imaging and multivariate data analysis. *Sensors 13*, 8916-8927.

Kritzinger, I., Lötze, E. & Jooste, M. (2017). Stone hardening and broken stones in Japanese plums (*Prunus salicina* Lindl.) evaluated by means of computed tomography scans. *Scientia Horticulturae 221*, 1–9

Leiva-Valenzuela, G.A., Lu, R. & Aguilera, J.M. (2014). Assessment of internal quality of blueberries using hyperspectral transmittance and reflectance images with whole spectra or selected wavelengths. *Innovative Food Science and Emerging Technologies 24*, 2–13

Li, B., Hou, B., Zhang, D., Zhou, Y., Zhao, M., Hong, R. & Huang, Y. (2016). Pears characteristics (soluble solids content and firmness prediction, varieties) testing methods based on visible-near infrared hyperspectral imaging. *Optik 127*, 2624-2630.

Liu, C., Liu, W., Chen,W., Yang, J. & Zheng, L. (2015). Feasibility in multispectral imaging for predicting the content of bioactive compounds in intact tomato fruit. *Food Chemistry 173*, 482-488.

Lorente, D., Aleixos, N., Gomez-Sanchis, J., Cubero, S., García-Navarrete, O.L., Blasco, J., (2012). Recent advances and applications of hyperspectral imaging for fruit and vegetable quality assessment. *Food Bioprocess and Technology 5*, 1121-1142.

Lu, R. & Peng, Y. (2006). Hyperspectral scattering for assessing peach fruit firmness. *Biosystems Engineering 93*, 161-171.

Mobaraki, N. & Amigo, J.M. (2018). HYPER-Tools. A graphical user-friendly interface for hyperspectral image analysis. *Chemometrics and Intelligent Laboratory Systems 172*, 174-187.

Munera, S., Amigo, J.M., Aleixos, N., Talens, P., Cubero, S. & Blasco, J. (2018). Potential of VIS-NIR hyperspectral imaging and chemometric methods to identify similar cultivars of nectarine. *Food Control 86*, 1-10

Munera, S., Amigo, J.M., Blasco, J., Cubero, S., Talens, P. & Aleixos, N. (2017). Ripeness monitoring of two cultivars of nectarine using VIS-NIR hyperspectral reflectance imaging. *Journal of Food Engineering 214*, 29-39

Nakano, R., Akimoto, H., Fukuda, F., Kawai, T., Ushijima, K., Fukamatsu, Y., Kubo, Y., 1, Fujii, Y., Hirano, K., Morinaga, K. & Sakurai, N. (2018). Nondestructive detection of split pit in peaches using an acoustic vibration method. *The Horticulture Journal 87*, 281–287.

Nicolaï, B.M., Beullens, K., Bobelyn, E., Peirs, A., Saeys, W., Theron, I.K., & Lammertyn, J., (2007). Non-destructive measurement of fruit and vegetable quality by means of NIR spectroscopy: a review. *Postharvest Biology and Technology* 46, 99–118

Nørgaard, L., Saudland, A., Wagner, J., Nielsen, J.P., Munck, L. & and Engelsen, S.B. (2000). Interval Partial Least-Squares Regression (iPLS): A Comparative Chemometric Study with an Example from Near-Infrared Spectroscopy. Society for Applied Spectroscopy 54, 413-419

Qin, J. & Lu, R. (2005). Detection of pits in tart cherries by hyperspectral transmission imaging. *Transactions of the ASAE*, 48, 1963-1970.

Qin, J., Chao, K., Kim, M.S., Lu, R. & Burks, T.F. (2013). Hyperspectral and multispectral imaging for evaluating food safety and quality. *Journal of Food Engineering 118*, 157-171.

Rajkumar, P., Wang, N., EImasry, G., Raghavan, G.S.V. & Gariepy, Y. (2012). Studies on banana fruit quality and maturity stages using hyperspectral imaging. *Journal of Food Engineering 108*, 194-200.

Reig, G., Alegre, S., Gatius, F. & Iglesias, I. (2013). Agronomical performance under Mediterranean climatic conditions among peach [Prunus persica (L.) Batsch] cultivars originated from different breeding programs. *Scientia Horticulturae 150*, 267-277.

Rinnan, Å., van den Berg, F., & Engelsen, S. B. (2009). Review of the most common pre-processing techniques for near-infrared spectra. *Trends in Analytical Chemistry 28*, 1201-1222.

Schaare, P.N. & Fraser, D.G. (2000) Comparison of reflectance, interactance and transmission modes of visible-near infrared spectroscopy for measuring internal properties of kiwifruit (*Actinidia chinensis*). *Postharvest Biology and Technology 20*, 175 – 184.

Schmilovitch, Z., Ignat, T., Alchanatis, V., Gatker, J., Ostrovsky, V. & Felfoldi, J. (2014). Hyperspectral imaging of intact bell peppers. *Biosystems Engineering 117*, 83-93.

Siedliska, A., Baranowski, P., Zubik, M. & Mazurek, W. (2017). Detection of pits in fresh and frozen cherries using a hyperspectral system in transmittance mode. *Journal of Food Engineering 215*, 61-71

Tani, E., Polidoros, A.N., & Tsaftaris, A.S. (2007). Characterization and expression analysis of FRUITFULL-and SHATTER-PROOF-like genes from peach (*Prunus persica*) and their role in split-pit formation. Tree physiology, 27, 649-659.

Valero, C., Crisosto, C.H. & Slaughter, D. (2007). Relationship between non-destructive firmness measurements and commercially important ripening fruit stages for peaches, nectarines and plums. *Postharvest Biology and Technology 44*, 248-253.

Williams, P. J., & Kucheryavskiy, S. (2016). Classification of maize kernels using NIR hyperspectral imaging. *Food Chemistry 209*, 131-138.

Williams, P.C. (1987). Variables affecting near-infrared reflectance spectroscopic analysis. In: Williams, P., Norris, K. (Eds.), Near-infrared Technology in the Agricultural and Food Industries. American Association of Cereal Chemists, St. Paul, MN, pp. 143-166.

Zhang, C., Guo, C., Liu, F., Kong, W., He, Y. & Lou, B. (2016). Hyperspectral imaging analysis for ripeness evaluation of strawberry with support vector machine. *Journal of Food Engineering 179*, 11-18.

Zhu, N., Lin, M., Nie, Y., Wu, D. & Chen, K. (2016). Study on the quantitative measurement of firmness distribution maps at the pixel level inside peach pulp. *Computers and Electronics in Agriculture 130*, 48-56.

FIGURES

Figure 1. Example of nectarine with split pit defect

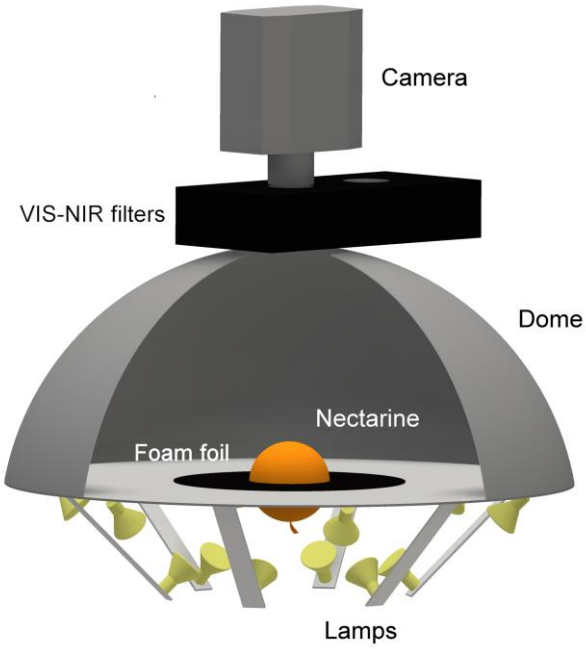

Figure 2. Hyperspectral acquisition system

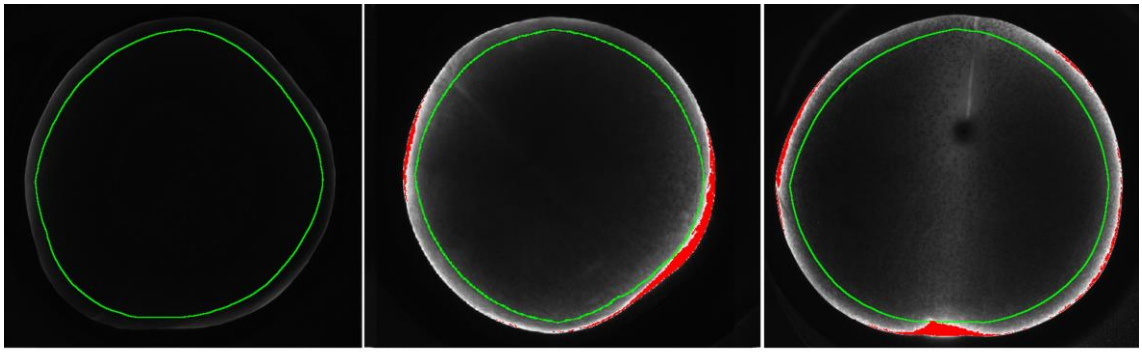

Figure 3. Image processing to select the ROI of each type of fruit: less ripe fruit (A), riper fruit (B) and split pit fruit (C).

Green line = limit of the ROI (analysed area); red pixels = saturated pixels

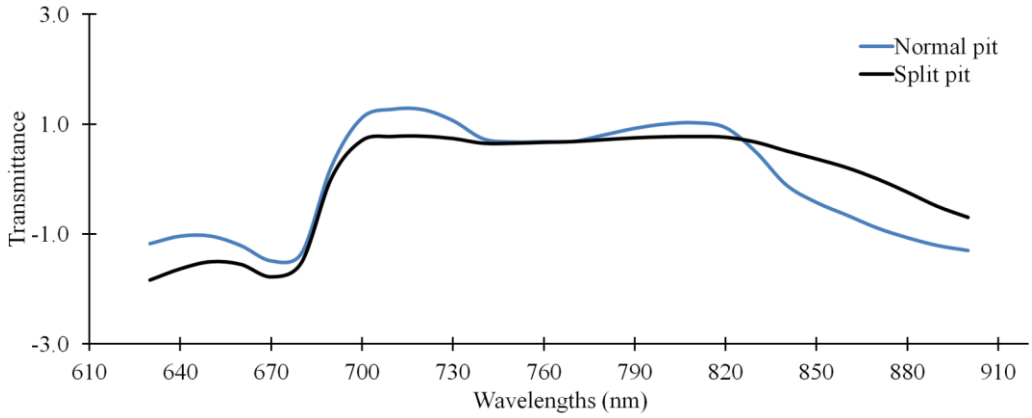

Figure 4. Mean spectra of 'Big Top' fruits with normal and split pit.

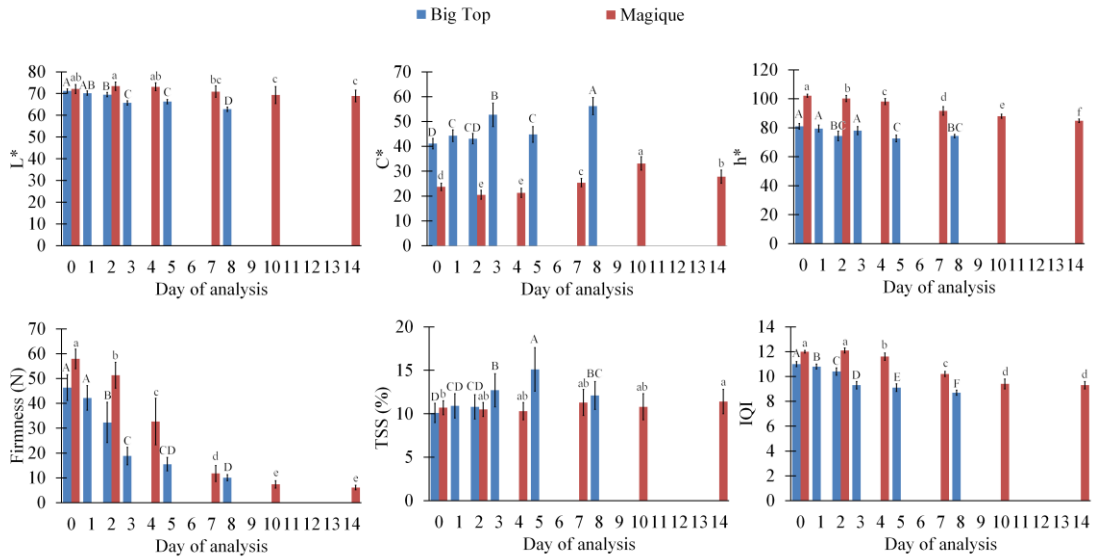

Figure 5. Results of the analysis of the reference quality parameters.

Columns are mean and bars are standard deviation. Different letters in each nectarine cultivar set indicate significant differences between groups (p-value<0.05), according to Tukey's (HSD) test.

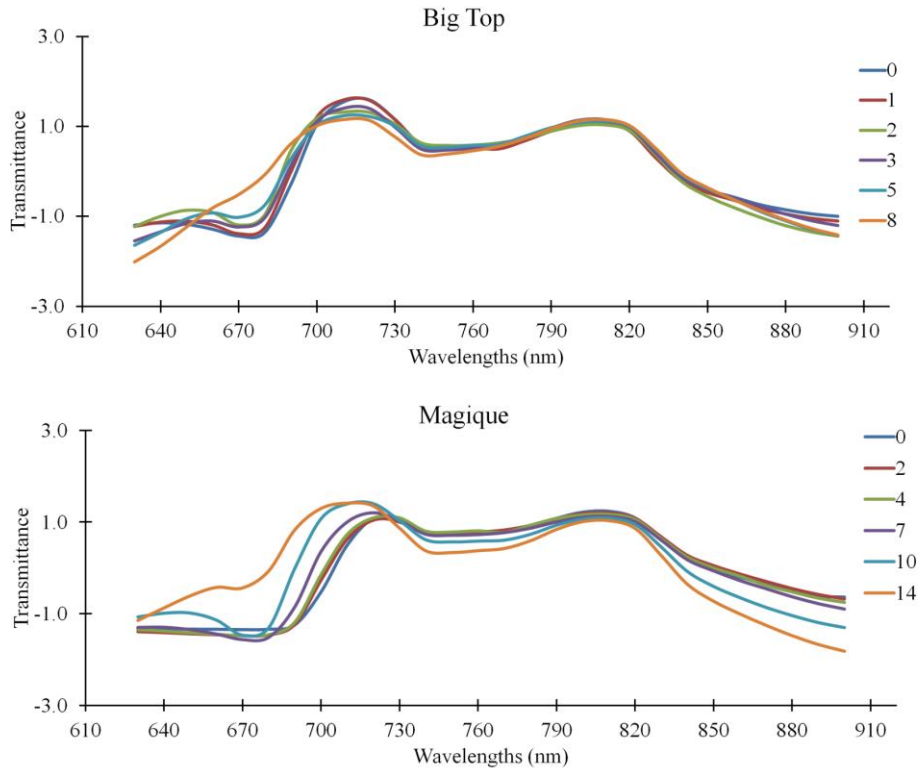

Figure 6. Mean spectra of the fruits of the 'Big Top' and 'Magique' cultivars on each day of analysis.

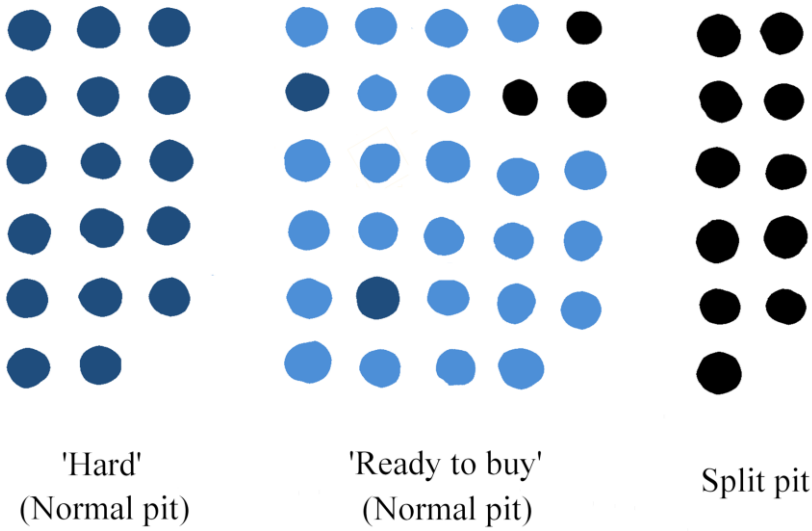

Figure 7. Visual verification of the hierarchical classification of the test set of 'Big Top' nectarines.